International Journal of Heat and Mass Transfer 52 (2009) 564–573

Contents lists available at ScienceDirect

International Journal of Heat and Mass Transfer

journal homepage: www.elsevier.com/locate/ijhmt

Gold nanoshell density variation with laser power for induced hyperthermia

Jerry Vera, Yildiz Bayazitoglu *

Department of Mechanical Engineering and Materials Science, Rice University, 6100 Main Street, MS 321, Houston, TX 77005-1892, USA

ARTICLE INFO

Article history:
Received 19 May 2008
Received in revised form 23 June 2008
Available online 25 August 2008

Keywords:
Photothermal therapy
Hyperthermia
Lasers
Nanoshell
Cancer therapy
Tissue optics

ABSTRACT

The thermal profile effects of nanoshell density, laser power, and laser arrangement are presented for ideal cases of nanoshell-assisted photothermal therapy. A one-dimensional thermal model utilizing the P_1 approximation is used to simulate the penetration of laser radiation and subsequent heating of 1-cm slabs of nanoshell-embedded tissue exposed to a 633-nm collimated light source. It is shown that adding too many nanoshells or increasing power can cause overheating in the entry region while leaving the rear region heated only by conduction, producing an undesirable temperature differential. An opposing dual-laser approach is presented that mitigates this issue.

1. Introduction

Over the past several years, much interest has been generated surrounding the use of light-absorbing gold nanoshells as a new tool to fight cancer using photothermal tumor therapy. It has been repeatedly shown that by varying the relative dimensions of the cores and thickness of the shell in such nanoparticles, the optical resonance can be precisely and systematically varied over a broad region ranging from the near-UV to the mid-infrared. This region includes the near-infrared (NIR) wavelength range where tissue transmissivity peaks [1–3]. By tuning gold nanoshells to maximize plasmon resonance, in this region these particles can efficiently absorb incident radiation and generate heat, which in turn raises the temperature of their immediate surroundings. Using any of a variety of means of injecting gold nanoshells into biological tissue, one can increase the temperature of the tissue by exposing a nanoshell-embedded tissue "composite" to laser light via minimally invasive fiber optics, and with increased absorption focused in those regions containing nanoshells, hyperthermia can be achieved in target areas with minimal consequence to non-nanoshell-embedded tissue [4]. Specifically, this procedure can be used to produce hyperthermia in malignant tumors with the goal of locally inducing cellular necrosis or weakening tumorous tissue into a state where necrosis can occur using a lower required dose of ionizing radiation from radiation therapy [5]. Because gold is considered a biocompatible material [3], this procedure is thus far considered safe, and both methods of inducing necrosis are favorable to traditional radiation therapy, where the DNA of all cells in the path of the radiation beam are subject to damage.

The purpose of this study is to investigate the feasibility of gold nanoshell-assisted photothermal therapy by focusing on the mechanical aspects of the problem: namely radiative transport, distributed heating, and thermal conduction. A simulation of optical diffusion based on radiative transport theory using the P_1 approximation in a solid medium with homogenously distributed gold nanoshells is used and applied to biological tissue as the base medium. Using a code developed by Bayazitoglu et al., several cases are presented of laser diffusion through and the subsequent heating of biological tissue infused with various gold nanoshell distribution densities. This study also simulates the heat distribution as a result of varying input power levels and reports the resulting temperature distributions at subsequent gradations of time. The goal is to present key examples of those parameters that would be required to raise a tissue to a given elevated temperature characteristic of hyperthermia while maintaining that the affected tissue is warmed evenly and steadily across its depth. Also noted is the time progression of this increase in temperature so that methods of raising and holding a tissue to a given hyperthermic state for a given time duration can be devised and utilized by therapists in the field of oncology.

2. Analysis

Previous studies have shown that a semitransparent medium can be engineered by embedding gold nanoshells in a transparent

* Corresponding author. Tel.: +1 713 348 6291.
E-mail address: bayaz@rice.edu (Y. Bayazitoglu).

0017-9310/$ - see front matter © 2008 Elsevier Ltd. All rights reserved.
doi:10.1016/j.ijheatmasstransfer.2008.06.036

Nomenclature

Symbols

B's	analytical constants
Bi	Biot number
C's	analytical constants
c	specific heat (J/kg K)
Fo	Fourier number
G	irradiance (W/m^2)
h	convective heat transfer coefficient (W/m^2 K)
I	intensity of radiation
k	thermal conductivity (W/m K)
L	length of slab
M	number of nodes
N_T	number of particles per unit volume or particle concentration (particles/m^3)
Q	efficiency
q	heat flux (W/m^2)
r_i	nanoshell core radius
r_o	nanoshell shell radius
T	temperature (°C or K)
ΔT	difference between highest and lowest temperature in target tissue region
t	time (s)
Δt	time increment (s)
u'''	heat generation (W/m^3)
z	axis of coordinate system inside medium pointing towards the depth normal to boundary (m)
Δz	spatial increment (m)

Greek symbols

α	thermal diffusivity (m^2/s)
β	extinction coefficient (m^{-1})
κ	absorption coefficient (m^{-1})
μ_c	$\cos\theta$
θ	laser angle of incidence
ρ	density (kg/m^3)
ρ	reflectivity
σ_s	scattering coefficient (m^{-1})
τ	optical depth or optical location
τ_L	optical length
ω	scattering albedo
ξ_1	analytical constant

Subscripts

c	correspond to collimated radiation
d	correspond to diffuse radiation
in	correspond to input
md	correspond to host medium
R	correspond to total radiation, summation of diffuse and collimated radiation
s	correspond to nanoshells
tot	correspond to total properties for nanoshell/host medium composite

Greek subscripts

β	correspond to extinction
κ	correspond to absorption
λ	spectral
σ	correspond to scattering

slab, and altering the number of nanoshells spread homogeneously throughout this slab can vary the levels of attenuation of light penetrating through this medium, which in turn varies the amount of absorption and heating made in the composite along its depth [6]. When light enters a nanoshell-embedded slab, propagating light is absorbed and scattered by both the host medium and the embedded nanoshells. The extent of absorption and scattering made by these two constituents can be analyzed linearly, since radiative transfer theory shows radiative intensity of a propagating light through an absorbing and isotropically scattering, one-dimensional plane parallel medium with constant radiative properties is a linear function [7]. Cases where nanoshell density is high, and inter-nanoshell distance is within a few particle diameters of one another are not considered here, since induced dipole–dipole interactions between neighboring nanoparticles will induce non-linear near-field effects [8].

2.1. Problem description

In this study, a collimated light source illuminates a 1-cm slab of human biological tissue with varying degrees of nanoshell densities homogeneously distributed within. In a clinical setting, the nanoshells are assumed to be added either by direct injection onto the site of interest, or intravenously with eventual deposition into the desired region due to vasculature abnormalities in tumorous tissue [9]. This slab represents what would be a pea-sized tumor that has developed within a healthy tissue, and it is surrounded on both sides by regions of healthy tissue. These regions provide a thermal conduction buffer zone which acts as a limited heat sink, without which temperatures in the illuminated tissue would escalate to higher than accurate levels. These are 1-cm long each and are located to the left and right of the nanoshell-embedded tissue.

The heat source assumed here is a 633-nm helium-neon laser delivered by a fiber optic cable that is inserted into the body in a minimally invasive procedure, is applied directly onto the site of a tumor, and projects into the direction of its depth. This projection is located on one end of the slab in the first round of studies and then on the two opposing ends of the slab in the second round of studies (see Fig. 1). A wavelength of 633 nm was chosen since absorption due to whole blood and water is low at this value, thus allowing for high transmissivity [10]. It is not surprising that as a result, the vast majority of tissue properties readily found in the literature were listed at this wavelength or at 1035 nm where absorption by these constituents is at a minimum [11].

Several types of tissue are examined including human brain, breast, subcutaneous fat, liver, and skin. The optical and thermal properties of these tissues are pertinent to the penetration of light and the subsequent heating and spread of heat throughout the slab depth. The tissue properties utilized are listed in Table 1. They were recorded at room temperature, and for the purpose of simplicity in the current analysis, they are assumed to remain constant as the temperature changes.

Nanoshells are added to the matrix in each of the tissues above with varying particle distribution densities, N_T, varying between 0, 7×10^{14}, 7×10^{15}, and 7×10^{16} particles per cubic meter. Studying the tissue optical properties listed in Table 1, we can see that in all cases, the absorption per unit length is relatively low in comparison to the scattering. As a result, the goal of the addition of the nanoshells to the matrix is to augment the amount of absorption that occurs in the tissue while keeping any additional scattering to a minimum. To accomplish this, a suitable nanoshell geometry

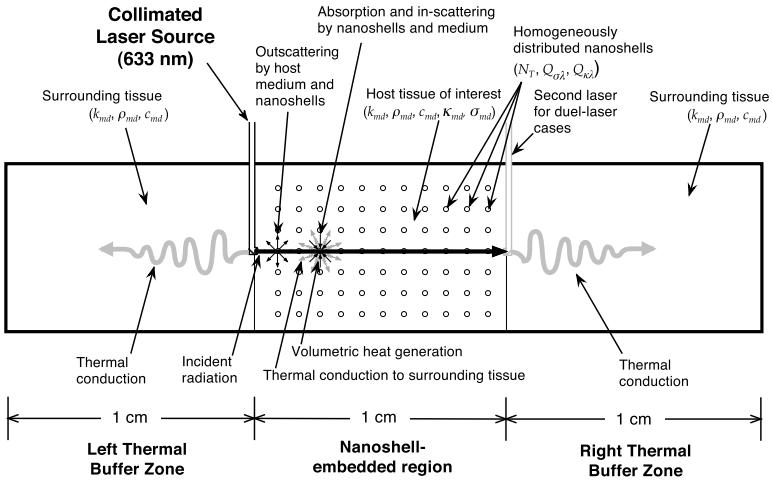

Fig. 1. One-dimensional nanoshell-embedded tissue thermal analysis setup.

Table 1
Utilized tissue thermal and optical properties at 633 nm

Tissue	Temperature (°C)	Index of refraction	Conductivity (W/m K)	Specific heat (J/kg K)	Mass density (kg/m^3)	Abs (m^{-1}) at 633 nm	Sca (m^{-1}) at 633 nm
Brain, human	37	1.37	0.515	3600	1035	26	5700
Breast, human	37	1.44	0.499	3920	990	20	39,400
Fat, subcutaneous	37	1.44	0.25	3920	916	10	6690
Liver, human	37	1.367	0.497	3600	1050	320	41,100
Skin, dermis	37	1.55	0.293	3150	1100	180	39,400

Estimates and substitutions used where needed. Source: Refs. [10–12].

is selected to target peak absorption and exhibit minimal scattering when exposed to a 633-nm excitation.

The extinction efficiency spectra of nanoshells can be calculated quite accurately using Mie theory [13]. After modeling several combinations of nanoshell core sizes and shell thicknesses, it was found that a nanoshell with a core radius of 16 nm and shell thickness of 5 nm produces desirable results. The absorption and scattering efficiency spectra of such a shell is shown in Fig. 2. This spectra is based on a Mie scattering approximation of an array of gold nanoshells surrounded by water with a two sigma Gaussian distribution between ±2 nm for r_1 and ±0.5 nm for the shell thickness. The variation in shell thickness and core size is used to factor in for a likelihood of polydispersity in the nanoshell suspension, and the inclusion of a surrounding medium is necessary to form the boundary conditions used in the Mie calculations. Water was chosen because it was deemed the closest approximation to tissue, which has a high water content, however, it should be noted that the resulting extinction spectra calculated by this method does not include absorption lines caused by water.

The nanoparticle spectral absorption and scattering cross-sections $\kappa_{s\lambda}$ and $\sigma_{s\lambda}$, respectively, are deduced from the spectral absorption and scattering efficiencies of the nanoshells $Q_{\sigma\lambda}$ and $Q_{\kappa\lambda}$ under the following relations:

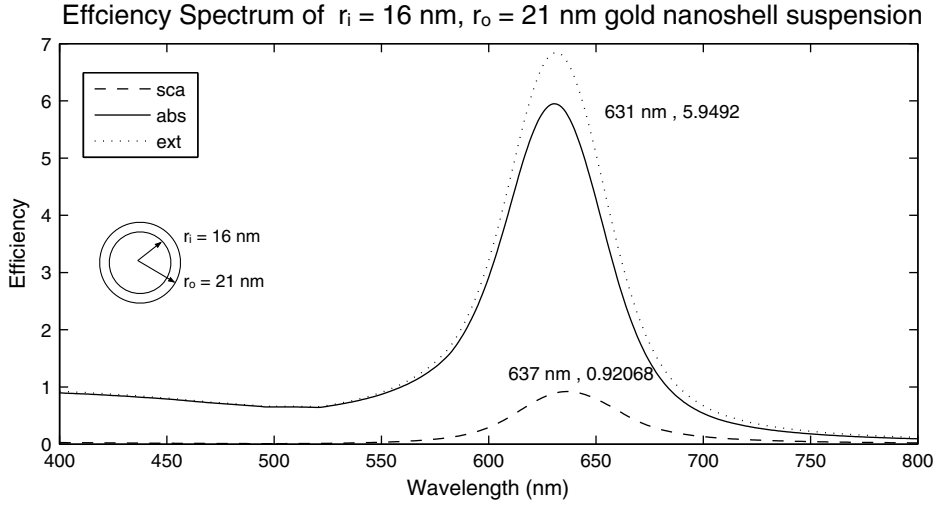

Fig. 2. Scattering and absorption spectra of $[r_i, r_o] = [16\,\text{nm}, 21\,\text{nm}]$ nanoshell suspension from Mie theory approximation with line broadening due to likely polydispersity in shell population.

$$\sigma_{s\lambda} = \pi r_o^2 Q_{\sigma\lambda} N_T \quad (1)$$

$$\kappa_{s\lambda} = \pi r_o^2 Q_{\kappa\lambda} N_T \quad (2)$$

again, where N_T is the number of nanoshells per unit volume. The absorption and scattering cross-sections in Eqs. (1) and (2) define the degree of absorption or scattering performed on the incoming light per unit depth at a particular wavelength by the nanoshell array. Increasing the density of nanoshells in the array increases the respective absorption and scattering. Increasing the nanoparticle cross-sectional area will have the same effect, however in the present study, nanoparticle efficiency is emphasized, therefore the optical properties and the geometry detailed in Fig. 2 is held constant, and only changes in distribution density are considered.

As noted, the tissue optical properties listed in Table 2 denote the respective absorption and scattering of the tissue alone at 633 nm. To model the combined extinction caused from the synthesis of both media, we apply a superposition principal stating that the combined extinction from the nanoshell-embedded tissue medium is equal to the sum of the extinctions from its constituent parts. The extinction cross-section is defined as the sum of the absorption and scattering cross-sections of a medium [7]. Here we have contributions to extinction from the nanoshell array and the host tissue in which they are dispersed. When broken down into their absorptive and scattering components, we have the following:

$$\begin{aligned}\beta_{\mathrm{tot}-\lambda} &= \beta_{s\lambda} + \beta_{md-\lambda} \\ \beta_{\mathrm{tot}-\lambda} &= \kappa_{s\lambda} + \sigma_{s\lambda} + \kappa_{md-\lambda} + \sigma_{md-\lambda} \\ \beta_{\mathrm{tot}-\lambda} &= \pi r_o^2 Q_{\kappa\lambda} N_T + \pi r_o^2 Q_{\sigma\lambda} N_T + \kappa_{md-\lambda} + \sigma_{md-\lambda}\end{aligned} \quad (3a, b, c)$$

The relative distinction between scattering and absorption is expressed in the scattering albedo for the composite system:

$$\omega_{\mathrm{tot}-\lambda} = \frac{\sigma_{\mathrm{tot}-\lambda}}{\beta_{\mathrm{tot}-\lambda}} \quad (4)$$

where the spectral scattering coefficient for the total composite system can be expressed as

$$\sigma_{\mathrm{tot}-\lambda} = \sigma_{s-\lambda} + \sigma_{md-\lambda} \quad (5)$$

we have the following relation for the total composite scattering albedo:

$$\omega_{\mathrm{tot}-\lambda} = \frac{\sigma_{s\lambda} + \sigma_{md-\lambda}}{\pi r_o^2 Q_{\kappa\lambda} N_T + \pi r_o^2 Q_{\sigma\lambda} N_T + \kappa_{md-\lambda} + \sigma_{md-\lambda}} \quad (6)$$

The scattering albedo here is used in the P_1 approximation shown in the following section to approximate the resulting collimated and diffuse incident radiation and heat flux as functions of optical depth into the medium. The heat flux profile is subsequently used to generate the time-dependent temperature profile.

2.2. Radiative analysis

To model the diffusion of light intensity, the solution to the near infrared heating of a one-dimensional, conducting and radiatively participating medium as presented in [6] is utilized. The assumptions taken here are nearly identical in that: (1) the medium is one-dimensional, (2) emission from the medium and nanoshells is negligible, (3) the host medium is homogeneous, (4) the gold nanoshells in the medium are distributed evenly, and (5) all of the nanoshells in the medium have the same size and aspect ratio (core diameter/shell diameter). This study differs where the host medium is assumed to be transparent to spectral irradiation, since the tissue media utilized here possess inherent absorption and scattering.

This solution uses the P_1 approximation described by Modest in [7]. As shown in [6], it manifests itself as a relation between the diffuse intensity of radiation with diffuse irradiance $G(\tau)$ and diffuse radiative heat flux $q(\tau)$ as functions of optical depth. The solution for the radiative heat flux profile is borrowed and then used in the FTDT analysis described in the next section to as a volumetric heating term that varies along the depth of the medium.

2.3. FDTD formulation

A finite difference time domain (FDTD) calculation is performed on the entire length of the tissue calculating the local temperature evolution over time. As stated, it is assumed that a fiber optic cable is inserted into the body during a minimally invasive procedure, and laser power is applied directly onto the site of a tumor, with entry of collimated radiation on one end of the slab in the first round of studies, then entry from the two opposing ends of the slab in the second round of studies.

Five assumptions are made in solving the temperature distribution: (1) the physical and thermal properties of the host medium are constant, (2) the nanoshells contribute negligible additional effects to the physical and thermal properties of the medium, (3) the medium is considered homogeneous, (4) the medium is one-dimensional, and (5) emission is negligible. The energy equation incorporating these assumptions can be expressed as:

$$\frac{1}{\alpha_{md}}\frac{\mathrm{d}T}{\mathrm{d}t} = \frac{\mathrm{d}^2 T}{\mathrm{d}z^2}\frac{u'''}{k_{md}} \quad (7)$$

where u''' is the local heat generation spectrum across the depth of the slab created by the absorption of incident radiation into the composite. It is defined as the negative sign of the divergence of radiative heat flux, which is taken from the radiative heat transfer analysis.

Table 2
Analytical constants

B_1	$-\frac{1}{\mu_c}\frac{\omega_\lambda(1-\rho_\lambda(0))q_{in,\lambda}}{\frac{1}{\mu_c}-\xi_1^2}$	B_2	$2-\frac{\epsilon_\lambda}{(2-\epsilon_\lambda)(1-\omega_\lambda)}\xi_1$
B_3	$2+\frac{\epsilon_\lambda}{(2-\epsilon_\lambda)(1-\omega_\lambda)}\xi_1$	B_4	$-\left(2+\frac{\epsilon_\lambda}{(2-\epsilon_\lambda)(1-\omega_\lambda)}\frac{1}{\mu_c}\right)$
B_5	$-\frac{\epsilon_\lambda}{2-\epsilon_\lambda}\frac{\omega_\lambda}{1-\omega_\lambda}(1-\rho_\lambda(0))q_{in,\lambda}+\frac{4(1-\epsilon_\lambda)}{2-\epsilon_\lambda}H_{c0,\lambda}$	B_6	$-\left(2e^{\xi_1\tau_{L\lambda}+\frac{\epsilon_\lambda}{(2-\epsilon_\lambda)(1-\omega_\lambda)}}\xi_1 e^{\xi_1\tau_{L\lambda}}\right)$
B_7	$-2e^{\xi_1\tau_{L\lambda}+\frac{\epsilon_\lambda}{(2-\epsilon_\lambda)(1-\omega_\lambda)}}\xi_1 e^{-\xi_1-\tau_{L\lambda}}$	B_8	$-2e^{1\tau_{L\lambda}/\mu_c}-\frac{\epsilon_\lambda}{(2-\epsilon_\lambda)(1-\omega_\lambda)}\frac{e^{-\tau_{L\lambda}/\mu_c}}{\mu_c}$
B_9	$-\frac{\epsilon_\lambda}{2-\epsilon_\lambda}\frac{\omega_\lambda}{1-\omega_\lambda}(1-\rho_\lambda(0))q_{in,\lambda}e^{\frac{-\tau_{L\lambda}}{\mu_c}}+\frac{4(1-\epsilon_\lambda)}{2-\epsilon_\lambda}H_{cL,\lambda}$	ξ_1	$\sqrt{3(1-\omega_\lambda)}$

Table 3
Values utilized in FDTD formulation

Parameter	Value
L	0.01 m
M	83
Δz	0.00012048 m
Δt	0.05 s

$$u''' = -\frac{dq_{R\lambda}}{dz} \tag{8}$$

The local heat transfer spectrum is treated as an array of localized points of heat generation that raises the temperature of the immediate surroundings. The spectral radiative heat flux, $q_{R\lambda}(\tau)$, is derived from combining components from the heat generation caused by collimated radiation $q_{c\lambda}(\tau)$ and the heat generation caused by diffuse radiation $q_{d\lambda}$:

$$q_{R\lambda}(\tau) = q_{c\lambda}(\tau) + q_{d\lambda}(\tau) \tag{9}$$

The collimated component, is derived in as a function of input power, reflectivity, and incoming direction:

$$q_{c\lambda}(\tau) = (1-\rho)q_{in}e^{\frac{-\tau}{\mu_c}} \tag{10}$$

where the componential fraction due to the angle of incidence is

$$\mu_c = \cos\theta \tag{11}$$

In all cases presented here, the laser penetrates the tissue in a direction normal to the entry boundary, i.e. $\theta = 0$, therefore

$$q_{c\lambda}(\tau) = (1-\rho)q_{in}e^{-\tau} \tag{12}$$

The diffuse component is given as

$$q_{d\lambda}(\tau) = C_1 e^{\zeta_1 \tau} + C_2 e^{-\zeta_1 \tau} + B_1 e^{-\tau} \tag{13}$$

where C_1 and C_2 are analytical constants obtained by solving:

$$\begin{bmatrix} C_1 \\ C_2 \end{bmatrix} = \begin{bmatrix} B_2 & B_3 \\ B_6 & B_7 \end{bmatrix}^{-1} \begin{bmatrix} B_4B_1 & B_5 \\ B_8B_1 & B_9 \end{bmatrix} \tag{14}$$

The B's and ξ_1 constants are tabulated in Table 2.

For brevity, the scattering albedo in Eq. (6), $\omega_{tot-\lambda}$, is presented as ω_λ. The full derivation of Eq. (13) can be found in reference [6]. The final result is an equation for the spectral radiative heat flux $q_{R\lambda}(\tau)$ as a function of the optical depth τ. The optical depth is a function dependent on the total extinction coefficient $\beta_{tot-\lambda}$ as shown in Eq. (3-b), and the current location z along the one-dimensional axis into the slab:

$$\tau_\lambda = \beta_{tot-\lambda} z \tag{15}$$

The total optical depth $\tau_{\lambda L}$ is

$$\tau_{\lambda L} = \beta_{tot-\lambda} L \tag{16}$$

In MATLAB, $q_{R\lambda}(\tau)$ is expressed as an array of M nodes across the irradiated slab of total length L. The discretized length between each node is labeled as Δz and is calculated as

$$\Delta z = \frac{L}{M-1} \tag{17}$$

where L is measured in meters. Table 3 outlines the values used and calculated here.

Thus $q_{R\lambda}(\tau)$ is expressed as $q_{R\lambda}(z)_i$ in discretized space where z is the direction and i is the number of steps along the nodes of that direction indicating the length. The discretized spectral radiative heat flux function obtained here is then used in Eq. (8) and incorporated into the unsteady heat transfer equation in (7) to simulate the effects of distributed heating by a laser source entering at $z = 0$ and model the change in temperature. For the cases where there are two laser sources, one at $z = 0$ and the other at $z = L$, a symmetry and linear addition theorem is applied. A laser entering from the right side of homogeneous tissue is assumed to have the same optical effects as one entering from the left side. Thus, the results from the heat flux calculations from one side can be applied to the other. We apply this principle to u''', Eq. (8), the negative derivative of the heat flux function. The MATLAB function `fliplr` is used to create a new array $u_R'''(z)$ from $z = 0$ to $z = L$ that is essentially the same array with values counting backwards from $z = L$ to $z = 0$. The original array in (8) is renamed $u_L'''(z)$, and the summation relation is applied to form a new array, $u_{tot}'''(z)$:

$$u_{tot}'''(z) = u_L'''(z) + u_R'''(z) \tag{18}$$

The total heat generation spectrum in (18) conducts heat throughout the tissue and applied to (7), where the thermal diffusivity α_{md} of the medium is defined by:

$$\alpha_{md} = \frac{k_{md}}{\rho_{md}c_{md}} \tag{19}$$

For the FTDT analysis, the Fourier number of the system must be below the critical value of $Fo_{crit} = 0.50$. The Fourier number is defined by:

$$Fo = \alpha_{md}\Delta t \Delta z \tag{20}$$

The boundaries of this system are additional 0.01-m slabs on each side of the slab system exposed to laser irradiation. Heat is allowed to spread into this system as the center slab is irradiated. The boundary regions are assumed represent surrounding tissue around the tumor site in the body, and for the purposes of this analysis, they are assumed to be composed of the same material as the slab of interest, so the thermal properties are identical. However, the boundary regions are not exposed to radiation, and thus do not exhibit any localized heat generation.

At the ends of the two boundary regions, for simplicity, the code assumes a complete cutoff of the computational space. This is simulated using a convection model on the first and final nodes of the system where the Biot number is set equal to 0 due to a convective heat transfer coefficient, h, of 0.

$$B_i = \frac{h\Delta Z}{k_{md}} \tag{21}$$

As a result of the statements above, the FDTD model utilizing the discretized mode of (8) is divided into five computational regions: the left cutoff node, the left boundary region, the medium of interest region (the nanoshell composite slab), the right boundary region, and the right cutoff node. The equations used to model these regions are delineated in Table 4.

Table 4
Governing finite-difference equations for respective nodes

Nodes	Finite difference equation	Region	Nodal length	Length
1	$T_m^{t+1} = T_m^t + 2BiFo(T_\infty - T_m^t) + 2Fo(T_{m+1}^t - T_m^t)$	Left Cutoff Node	1	Point
2–81	$T_m^{t+1} = T_m^t + Fo(T_{m+1}^t + T_{m-1}^t - 2T_m^t)$	Left Buffer Zone	79	0.01 m
82–164	$T_m^{t+1} = T_m^t + Fo(T_{m+1}^t + T_{m-1}^t - 2T_m^t) - \frac{Fo(\Delta z)^2}{k_{md}}\beta_{total-\lambda}u_{fd}'''$	Irradiated Slab Region	82	0.01 m
165–249	$T_m^{t+1} = T_m^t + Fo(T_{m+1}^t + T_{m-1}^t - 2T_m^t)$	Right Buffer Zone	84	0.01 m
250	$T_m^{t+1} = T_m^t + 2BiFo(T_\infty - T_m^t) + 2Fo(T_{m-1}^t - T_m^t)$	Right Cutoff Node	1	Point

3. Results and discussion

Resulting time-dependent temperature profiles were prepared for all tissues presented using varying particle distribution densities, N_T, of nanoshells varying between 0, 7×10^{14}, 7×10^{15}, and 7×10^{16} particles per cubic meter. Using these densities and the nanoshell geometry and optical properties shown in Fig. 2, the maximum possible augmentation to the inherent scattering and absorption of the host tissues (Table 1) is shown by the tabulation in Table 5.

For every density variation, four power levels for the input laser beam were used: 5000 W/m^2, 10,000 W/m^2, 15,000 W/m^2, and 20,000 W/m^2. This process was done using a single laser from the left side at $z = 0$, and was repeated using a dual laser configuration at $z = 0$ and $z = L$, both facing each other, pointing into the nanoshell-embedded tissue.

The total results are too numerous to include here, so only the most significant findings are presented which showed the general trends found between all cases. In general, the change of the temperature profile were very similar between five major categories of variation. They are:

(1) increasing the nanoshell density distribution while holding power intensity constant,
(2) increasing the power intensity while holding the nanoshell density constant
(3) using two (dual) facing lasers as opposed to one single laser,
(4) using the dual-laser configuration and holding the nanoshell dispersion density constant and increasing the power, and
(5) using the dual-laser configuration and increasing the nanoshell density distribution while holding the power intensity constant.

Fig. 3 shows the effect of nanoshell density variation on a 0.01 cm slab of breast tissue. The graph is divided into three parts. The center shows the evolution of the temperature profile over time in the nanoshell-embedded region in increments of 5 min. This region represents the section of tissue heated by the laser. To the left and right of this section are the bordering tissue regions which represent the surrounding healthy tissue which warm by conduction.

Two metrics are used to quantify the change in heating of the temperature profile. The first is the time taken for the entry node ($z = 0$) to reach 55 °C. Fifty-five degree celcius was chosen since it is a higher temperature than most cases presented in the literature for hyperthermia, and it is considered an extreme upper bound for the cases presented. The second metric is the temperature difference between the highest and lowest temperatures induced in the central tissue region at the point in time where the entry note reaches 55 °C and the simulation stops. Since the general goal of induced hyperthermia is to raise the temperature of a desired region of tissue, it is advantageous for the elevated temperature distribution to be as even as possible. Thus, a high ΔT in the 1-cm targeted tissue region is undesirable. Efforts should be made to minimize this number. Furthermore, it is also desirable to leave the healthy surrounding tissue largely unaffected by the propagation of heat from the laser beam. Thus cases where the target region temperature goals are met while leaving temperatures in the left and right "buffer" zones relatively close to normal body temperature (36.8 °C) are preferred.

In Fig. 3, we see that the control tissue in (a) requires 50.3 min for the entry node to reach 55 °C and has a ΔT of 5.11 °C across the tissue in the region from 0.01 m to 0.02 m. It can be seen from the different profile lines at 5 min, 10 min, etc. that the ΔT slowly increases as time progresses, so if a desired temperature increase is

Table 5
Contribution to scattering and absorption by $[r_i, r_o] = [16, 21]$ nm nanoshells

Dispersion density (m^{-3})	Nanoshell area (m^2)	Absorption efficiency (m^{-1})	Scattering efficiency (m^{-1})	Shell absorption coefficient (m^{-1})	Shell scattering coefficient (m^{-1})
0	1.38544E−15	5.9492	0.92968	0	0.000
7.00E+14	1.38544E−15	5.9492	0.92968	5.770	0.902
7.00E+15	1.38544E−15	5.9492	0.92968	57.696	9.016
7.00E+16	1.38544E−15	5.9492	0.92968	576.959	90.161

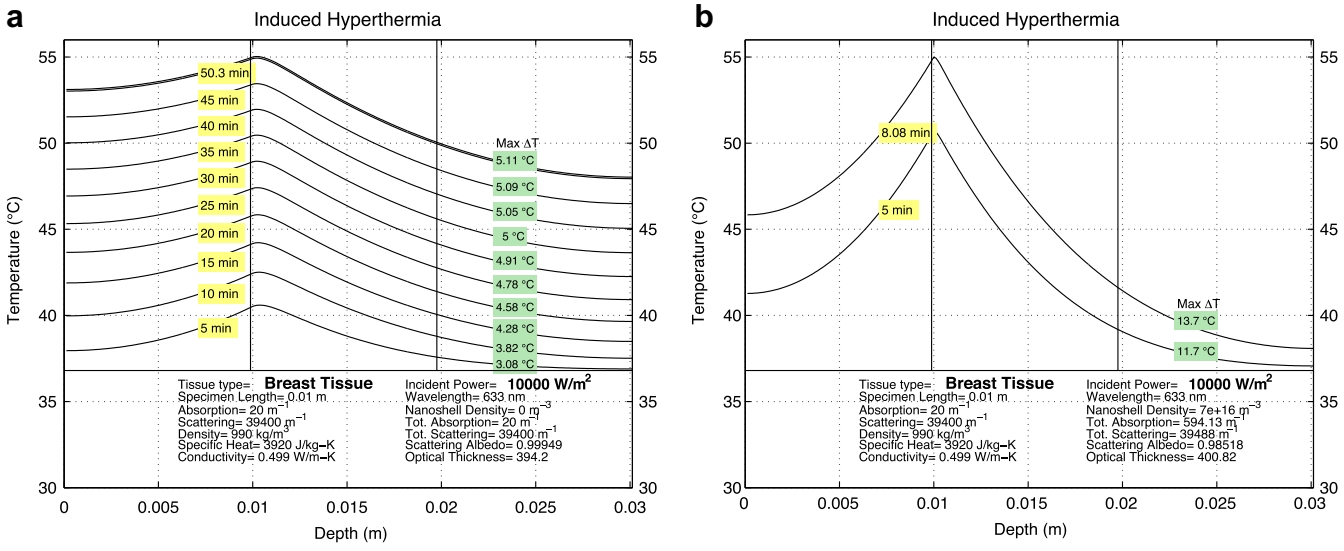

Fig. 3. Effect of increased nanoshell distribution density on induced hyperthermia for breast tissue at 10,000 W/m^2: (a) control tissue with zero nanoshell addition, (b) identical tissue with 7×10^{16} nanoshells/m^3.

only 45 °C, then it only requires between 15 and 20 min of heating time and the ΔT would be between 4.28 to 4.58 °C. One should also note that without nanoshells, the total absorption cross section in the targeted tissue region is only 20 m^{-1}. This explains the high heating time. The longer it takes for the tissue to heat to the desired temperature, the more time that is allowed for heat to propagate to the surrounding tissue via conduction. This is shown in (a), as the temperature 0.01 m to the left of central tissue region is 53 °C at 50.3 min, and the point 0.01 m to the right of the central region is as high as nearly 48 °C. Such broad heating is undesirable for this study, since we wish only to target the central region.

Raising the nanoshell content to 7×10^{16} particles per meter, shown in Fig. 3b, increases the total absorption coefficient nearly 30 times to 594.13 m^{-1}. This lowers the required heating time to 8.08 min, which is desirable, but it also increases the temperature differential across the 0.01-m central region to 13.7 °C.

Fig. 4 shows the effects of altering the laser power intensity while holding nanoshell distribution density constant. The tissue here is the dermis layer of human skin, with an inherent absorption coefficient of 180 m^{-1} and a scattering coefficient of 39,400 m^{-1}. The presence of nanoshells raises the absorption to 185 m^{-1} and the scattering to 39,401 m^{-1}. We can see that in the control case at 5000 W/m^2, shown in (a), 28.3 min is required to raise the tissue to 55 °C and the max ΔT is 10.1 °C. Raising the laser power while holding the nanoshell density constant lowers the required heating time to 9.28 min but increases the ΔT to 14.6 °C. The decrease in heating time is beneficial, since the warming of surrounding tissue is lowered, however the uneven temperature distribution results in a lack of heating to the rear region of the targeted central zone, where the temperature only reaches 41 °C.

Comparing Figs. 3b and 4b, it can been seen that despite differences in density, specific heat, and conductivity between breast tissue and skin dermis, the effects of adding nanoshells or increasing power density are very similar: both lower heating time while increasing ΔT. For the purposes of evenly heating a long section of tissue, both methods yield undesirable results.

When using two opposing lasers to heat the selected tissue region, however, the results improve. Fig. 5 shows the effect of altering the laser configuration while holding all other variables constant, using subcutaneous fatty tissue with 7×10^{14} nanoshells/m^3 density and a power level of 15,000 W/m^2. In (a), the control tissue requires 7.55 min for the entry point to reach 55 °C. The offset peak from the entry node to slightly inside the depth of the tissue is characteristic of the deeper penetration of incident radiation allowed by tissues of lower scattering, since the total scattering coefficient here is 6690.9 m^{-1} compared to ~39,000 m^{-1} as in the previous examples. Switching to two opposing lasers, shown in (b) lowers the required heating time to 5.5 min and lowers the maximum ΔT to 4.96 °C. In addition, the temperature drops off significantly in the surrounding tissue, making this combination highly attractive for the targeted heating of only the central region.

The effects of increasing power in the duel laser configuration is presented in Fig. 6. In (a) we see the control tissue, in this case, gray matter in the brain with no nanoshells present and heated at 5000 W/m^2. The inherent absorption is low, at 26 m^{-1} and the scattering is also relatively low, at 5700 m^{-1}. With these parameters, it takes 17.7 min to reach 55 °C, and the ΔT is low at 1.65 °C giving a highly even temperature distribution. This combination would be ideal except for the fact that the longer heating time also results in a high temperature in the surroundings. Increasing the power density, shown in (b), mitigates this issue. Raising the power density to 20,000 W/m^2 lowers the required heating time to 3.22 min and increases the maximum ΔT to 4.14 °C. The temperature peak is slightly inside the medium on both ends due to the relatively low scattering of 5700 m^{-3}. This causes the small disparity between the entry node where the laser light enters and the point of maximum temperature. Also, with this combination, the temperature of the surrounding tissue drops off quickly and remains relatively low. This favorable profile is achieved without the aid of nanoshells.

Fig. 7 looks at a case very similar, except it follows the effect of the increase of power in a tissue with inherently higher scattering. Here, human liver tissue with a scattering coefficient of 41,100 m^{-1} and absorption coefficient of 320 m^{-1} with no nanoshells is heated with dual 5000 W/m^2 lasers, then dual 15,000 W/m^2 lasers. In the first case, shown in (a), an intensity of 5000 W/m^2 yields a required time of 17.8 min and a max ΔT of 1.22 °C. Increasing the intensity to 15,000 W/m^2 in liver, shown in (b), has the same effect as it had in the gray matter in Fig. 6b, except we can see that the peaks are

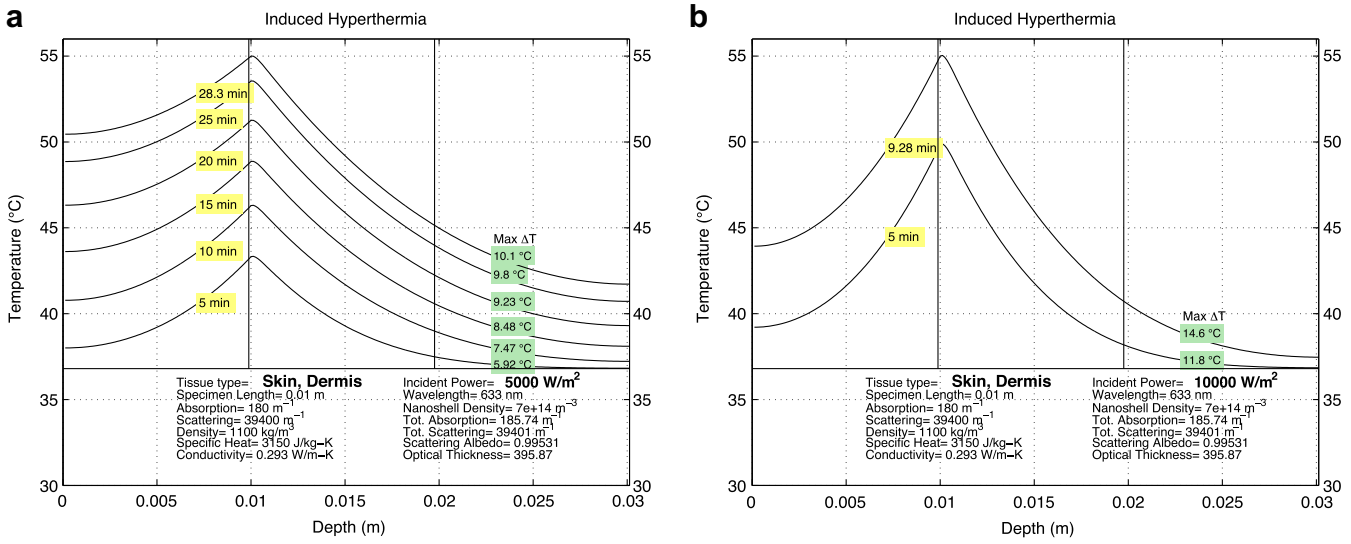

Fig. 4. Effect of increased power on induced hyperthermia for dermal skin tissue with 7×10^{14} nanoshells/m^3 density: (a) control tissue exposed to 5000 W/m^2 laser, (b) identical tissue exposed to 10,000 W/m^2 laser.

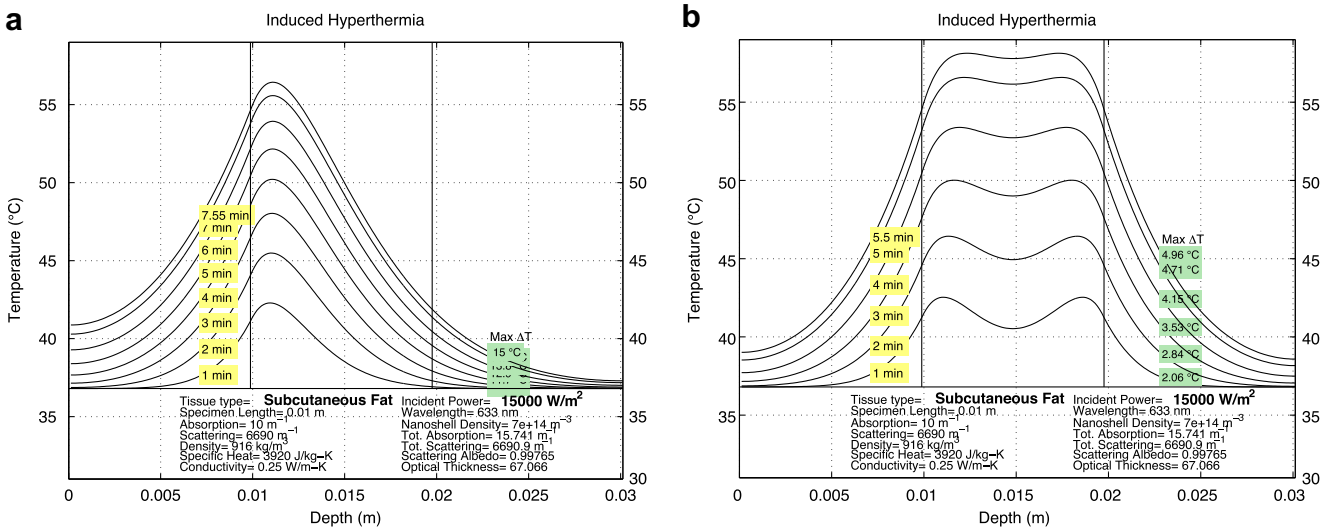

Fig. 5. Effect of use of duel lasers on induced hyperthermia for subcutaneous fatty tissue with 7×10^{14} nanoshells/m^3 density at 15,000 W/m^2: (a) control tissue exposed to single 15,000 W/m^2 laser, (b) identical tissue exposed to two opposing 15,000 W/m^2 lasers.

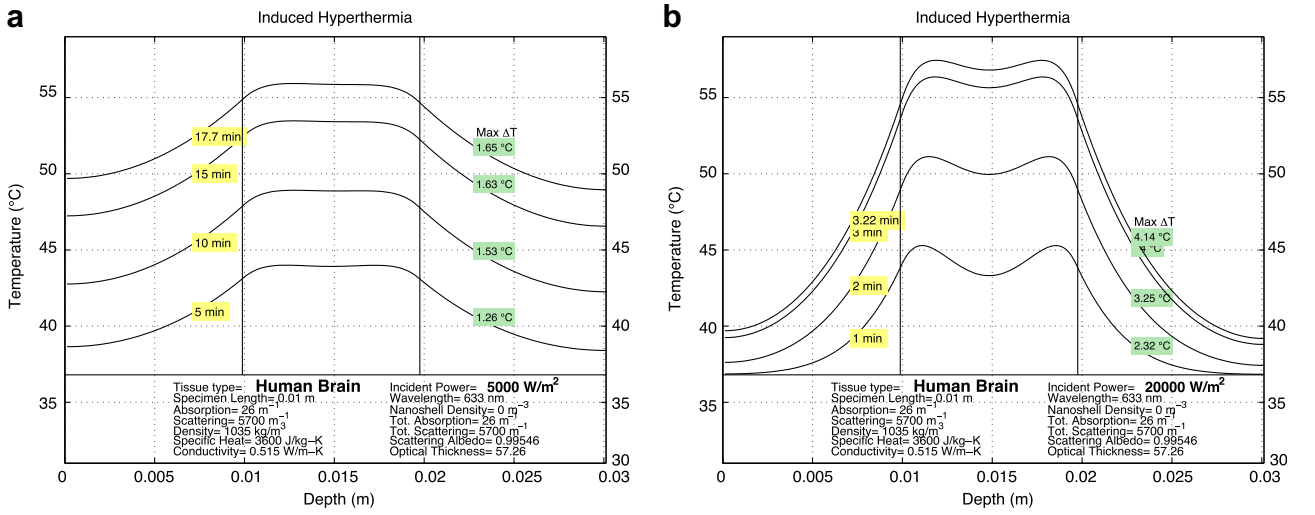

Fig. 6. Effect of increased power on induced hyperthermia for brain tissue with no nanoshell addition during use of duel lasers: (a) control tissue exposed to two opposing 5000 W/m^2 lasers, (b) identical tissue exposed to two opposing 20,000 W/m^2 lasers.

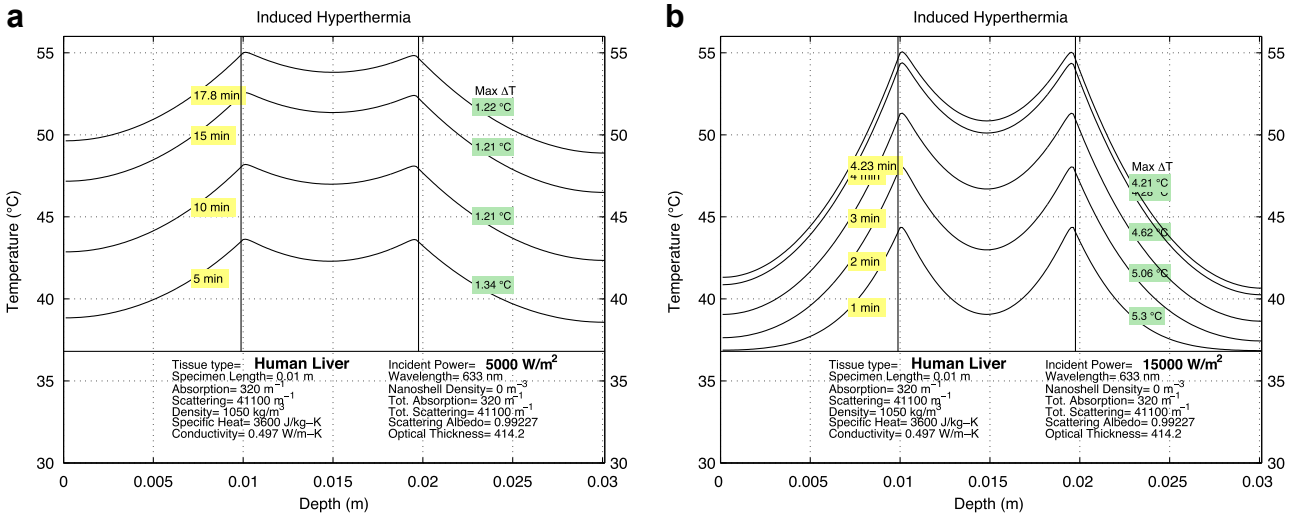

Fig. 7. Effect of increased power on induced hyperthermia for human liver tissue with no nanoshell addition during use of duel lasers: (a) control tissue exposed to two opposing 5000 W/m^2 lasers, (b) identical tissue exposed to two opposing 15,000 W/m^2 lasers.

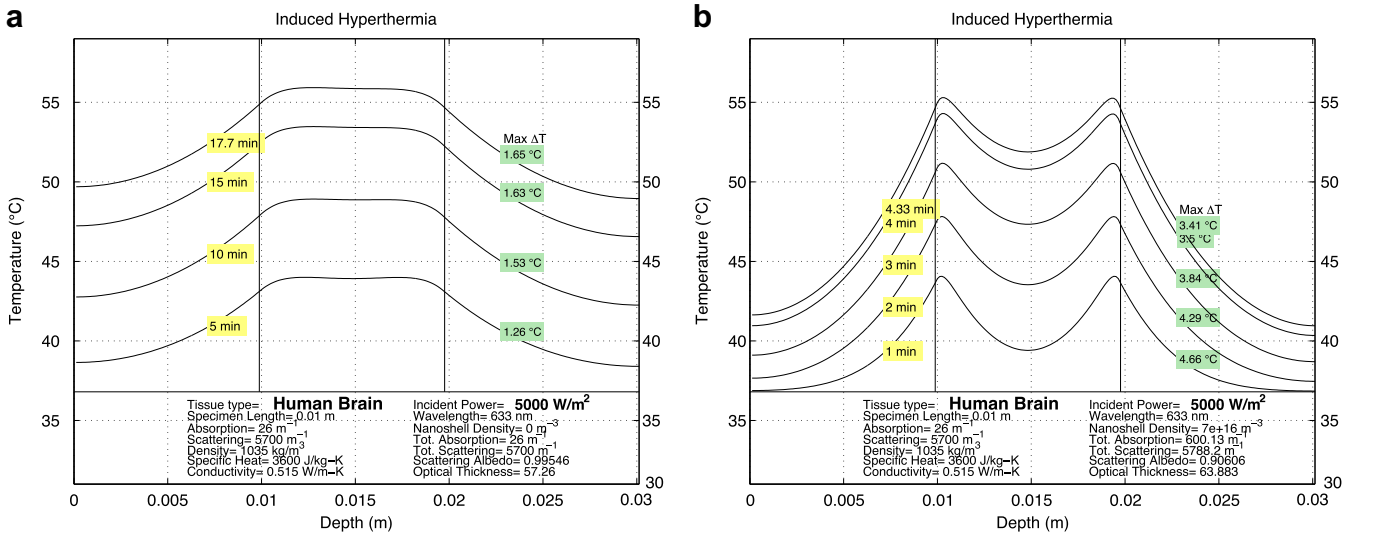

Fig. 8. Effect of increased nanoshell concentration on induced hyperthermia for human liver tissue at during use of duel 5000 W/m^2 lasers: (a) control tissue with no nanoshells, (b) identical tissue with 7×10^{16} nanoshells.

no longer shifted to the center, and the profile is not as smooth. The heating time is lowered to 4.23 min and the ΔT is 4.21 °C with the lowest temperature at the center.

Finally, the effect of nanoshell addition in a two-beam case without changing laser power is presented. For comparative purposes, human brain gray matter tissue is used again. In Fig. 8a, we see the same as Fig. 6a, gray matter with no nanoshells subject to intensive laser radiation of 5000 W/m^2 from opposing sides. Fig. 8b shows the effect of adding 7×10^{16} nanoshells/m^3 to the system. The results appear very similar to that in Fig. 7b: the required heating time is lowered to 4.33 min and the ΔT in the region of interest is moderately low at 3.41 °C. Also, the drop off of temperature in the surrounding tissue is almost identical.

4. Summary and conclusion

The effects of gold nanoshell distribution density, laser power intensity, and laser arrangement on induced hyperthermia for five different tissue types have been presented. It is assumed that the addition a nanoshell array to a tissue will create additional absorption or scattering that will supplement that inherent for a tissue at a given wavelength. Calculations were performed modeling the penetration of a 633-nm collimated light source using the P_1 approximation to obtain a spectral radiative heat flux profile for each case, assuming the tissue as an absorbing and isotropically scattering, one-dimensional plane parallel medium with constant radiative properties. An FDTD simulation utilizing these results was made to simulate the conductive propagation of heat through each tissue to generate a time-dependent temperature profile. The tissues analyzed were breast tissue, skin dermis, subcutaneous fat, liver, and gray matter tissue. For each, four nanoshell distribution densities, each at four power intensities, were tested where the irradiation process was simulated using one then two lasers. Heating commenced in each case until a stopping criteria of 55 °C in the entry node was reached. From the resultant temperature profiles obtained, patterns were observed showing that despite subtle differences in conductivity, specific heat, and density for all tissues, similar effects from the addition of nanoshells, the addition of laser intensity, or the modification of the laser arrangement – in particular, using two opposing lasers – could be seen, and a few examples could be chosen as representative samples to illustrate these effects. It can be seen that adding nanoshells or increasing the density of nanoshells in a sample significantly decreases the time required for heating. This is beneficial in cases were a small area is targeted for heating and it is desired to leave the surrounding region unaffected. However, this is not advantageous if a wider area is desired to be heated. The addition of nanoshells to a slab affectively increases the absorption and lowers the skin depth of the sample. As a result, the entry region of the slab where the laser first penetrates to absorbs most of the incoming radiation while leaving little or none to reach the deeper levels, and volumetric heating only occurs at the entry boundary leaving the rest of the tissue heated by thermal conduction. In addition, because of rapid heating at the entry, a highly uneven temperature profile develops because of less time for the heat to propagate before the entry reaches the established stopping criteria.

It can be seen that the addition of laser intensity (power density) has a similar effect. With an increased intensity, volumetric heating due to optical absorption in the entry region causes the temperature in this region to rise rapidly, allowing little time for heat to diffuse evenly into the tissue depth. Without the stopping criteria at 55 °C, temperatures at the entry would continue to escalate, and the entry region would undergo pyrolysis and ablation before the rest of the tissue could warm.

The use of two opposing lasers best suits the needs of even heating across a given depth. This can be achieved with or without the use of gold nanoshells. Rapid heating can be trigged by either increasing the power or increasing the nanoshell concentration. In such a configuration, rapid heating is beneficial, since little time is allowed for heat to spread to the surroundings, creating a plateau-like temperature profile with the highest temperatures produced in the target region. This is best achieved with tissues exhibiting lower scattering.

This study made several simplifying assumptions, including constant temperature thermal properties and the omission of blood-flow related effects. Additionally, for cancer therapy, tumorous tissues have been known to host different optical properties than those in their healthy state. Future studies incorporating such tissue data and blood flow effects as presented by the bio-heat equation are needed to increase accuracy. For the purposes of presenting the general effects of nanoshell addition, laser intensity, and laser configuration on irradiated samples of human tissue, however, this simplified model serves as a good starting point.

Acknowledgements

This work was funded by the Alliances for Graduate Education and the Professoriate (AGEP) program through the National Science Foundation Grant HRD-0450363. The kind guidance and assistance from Indra Tjahjono, Joseph Cole and the fruitful seminar series from the Laboratory for Nanophotonics (LANP) at Rice is also gratefully acknowledged.

References

[1] R.D. Averitt, S.L. Westcott, N.J. Halas, Linear optical properties of gold nanoshells, J. Opt. Soc. Am. B 16 (10) (1999) 1824–1832.
[2] Christopher Loo, Nanoshell-enabled photonics-based imaging and therapy of cancer, Technol. Cancer Res. Treat. 3 (1) (2004) 33–40.
[3] C. Loo, A. Lowery, N. Halas, J. West, R. Drezek, Immunotargeted nanoshells for integrated cancer imaging and therapy, Nano Lett. 5 (4) (2005) 709–711.
[4] Amanda R. Lowery, Immunonanoshells for targeted photothermal ablation of tumor cells, Int. J. Nanomed. I (2) (2006).
[5] P. Wust, Hyperthermia in combined treatment of cancer, Lancet Oncol. 3 (2002) 487–497.
[6] I. Tjahjono, Y. Bayazitoglu, Near-infrared light heating of a slab by embedded nanoparticles, Int. J. Heat Mass Transfer 51 (2008) 1505–1515.
[7] M. Modest, Radiative Heat Transfer, second ed., Academic Press, New York, 2003.
[8] D.W. Brandl, C. Oubre, P. Nordlander, Plasmon hybridization in nanoshell dimers, J. Chem. Phys. 123 (2005).
[9] A.M. Gobin, M.H. Lee, N.J. Halas, W.D. James, R.A. Drezek, J.L. West, Near-infrared resonant nanoshells for combined optical imaging and photothermal cancer therapy, Nano Lett. 7 (7) (2007) 1929–1934.
[10] Tuan Vo-Dinh (Ed.), Biomedical Photonics Handbook, CRC Press, Boca Roton, FL, 2003.
[11] Francis A. Duck, Physical Properties of Tissue: A Comprehensive Reference Book, Academic Press Inc., San Diego, 1990.
[12] W. Cheong, S.A. Prahl, A.J. Welch, A review of the optical properties of biological tissues, IEEE J. Quant. Electron. 26 (12) (1990) 2166–2185.
[13] S.J. Oldenburg et al., Nanoengineering of optical resonances, Chem. Phys. Lett. 288 (2–4) (1998) 243–247.